

Advancements in Temporal Fusion: A New Horizon for EEG-Based Motor Imagery Classification

Saran Kundu, Aman Singh Tomar, Anirban Chowdhury, *Member, IEEE*, Gargi Thakur, Aruna Tomar

Abstract—BCIs facilitate seamless engagement between individuals with motor disabilities and their surrounding environment by translating electroencephalography (EEG) signals generated from Motor Imagery (MI). Crucial to this process is the accurate classification of different types of MI tasks - a challenge that calls for the consistent evolution and refinement of reliable methodologies for EEG signal classification. This paper introduces three innovative approaches: M1, employing a temporal block technique combined with Filter Bank Common Spatial Pattern (FBCSP) and mutual information-based feature selection with a Random Forest classifier; and M2 and M3, extending M1 using Temporal Probability Fusion (TPF) and Probability Difference-based Temporal Fusion (PDTF) respectively. These methods aim to enhance MI EEG signal classification. The effectiveness of M1, M2, and M3 was scrutinized under differing scenarios including changing overlap sizes and channel choices. The analysis highlights that our methods exhibit enhanced performance under particular conditions, underlining the crucial role of temporal information and channel selection. Comparison with established methodologies verifies the superior efficiency of our proposed strategies. This study foregrounds the considerable potential of TPF and PDTF in MI EEG classification tasks, with significant implications for the future development of BCI systems.

Index Terms—Machine Learning, Motor Imagery Classification, EEG, Brain-Computer Interface (BCI), Temporal Probability Fusion (TPF), Probability Difference-based Temporal Fusion (PDTF), Temporal Block Approach, Neurorehabilitation.

I. INTRODUCTION

Brain-computer interfaces (BCIs) have received considerable attention in the past few decades due to their potential to assist individuals with severe motor disabilities, offering a new communication channel that does not require muscle movement [1], [2]. BCIs decipher and translate brain signals into commands to control external devices, such as wheelchairs [3], robotic arms [4], or computer cursors [5]. The key to successful BCI operation lies in accurately interpreting the brain's activity, and for this, the motor imagery (MI) paradigm has been widely adopted. MI refers to the mental rehearsal of motor actions without any overt movement or muscle activation [6].

Manuscript received XXXX XX, 2023; revised XXXX XX, 2023.
(Corresponding author: Aman Singh Tomar.)

S. Kundu is with CDAC, Noida, Guru Gobind Singh Indraprastha University, Delhi, India (e-mail: kundu.saran16@gmail.com). A. S. Tomar is with Kalyani Government Engineering College, WBUT, Kalyani, India (e-mail: amanast2000@yahoo.co.in). A. Chowdhury is with School of Computer Science and Electronic Engineering, University of Essex, Colchester, CO4 3SQ, UK (e-mail: a.chowdhury@essex.ac.uk). G. Thakur is with the Department of Networking and Communications, SRM Institute of Science and Technology Chennai, India (e-mail: gargilhzln@gmail.com). A. Tomar is with Department of Metallurgical and Materials Engineering, Indian Institute of Technology Roorkee, India (e-mail: arunadmt13@gmail.com.)

Motor imagery-based BCIs were first introduced by Ramoser, Müller-Gerking, and Pfurtscheller, who developed an optimal spatial filtering method for single-trial EEG during imagined hand movement [1]. This landmark study has since spurred many advancements in the field. Recent innovations include controlling quadcopters in three-dimensional space using a non-invasive MI-based BCI [6], which extends the application of BCIs to novel and practical real-world scenarios. For instance, Pichiorri et al. discussed the potential of BCI for motor and cognitive rehabilitation after stroke [7], while Philips et al. examined the use of topographical measures of functional connectivity as biomarkers for post-stroke motor recovery [7]. Furthermore, BCIs have been studied for dysphagia rehabilitation, with promising results [8].

Despite these advancements, several challenges remain in MI-based BCI, such as the inherent non-stationarity of EEG signals, the variability of user performance, and the requirement for extensive user training [6], [9]. To address these challenges, researchers have been exploring novel methodologies for improving the classification accuracy of MI tasks. Some researchers have used the temporal block-based approach to capture the temporal dynamics of MI-related EEG features using the sliding window technique on common spatial patterns and deep learning [10], [11] while some studies used feature selection to find optimal time window [12].

In this paper, we contribute to the evolving discourse by introducing two novel approaches: the Probability Difference-based Temporal Fusion (PDTF) approach and the Temporal Probability Fusion (TPF) approach. They use prediction probabilities and their differences over temporal windows for class label determination. Both methods aim to leverage the temporal dynamics of EEG signals and probabilistic classifier information to improve the classification of MI tasks.

The PDTF approach focuses on the use of prediction probabilities and their differences over temporal windows for class label determination. This technique capitalizes on the probabilistic information provided by the classifier to enhance the classification accuracy of MI tasks.

On the other hand, the TPF approach takes into consideration the weighted prediction probabilities of all temporal blocks belonging to a single trial for class label determination. This novel strategy seeks to further refine the classification process by assigning weights to predictions based on their temporal sequence, thus emphasizing the temporal structure of MI tasks.

This paper presents a comprehensive analysis of the PDTF and TPF approaches, demonstrating their potential to enhance MI-BCI performance and contribute to the broader BCI field,

including its application in rehabilitation contexts. Our findings underline the potential of these novel methodologies in improving the usability and effectiveness of MI-BCIs, driving forward our understanding and application of this transformative technology.

To provide a comprehensive understanding of the proposed approach, Section II provides an overview of related work in MI-EEG classification, while Section III details our proposed approach. In Section IV, we present the experimental results and discuss the findings, and in Section V, we conclude the paper and outline future research directions in this area.

II. BACKGROUND

In the realm of Brain-Computer Interfaces (BCIs), specifically, those based on Motor Imagery (MI), significant advancements have been made in terms of feature extraction and classification techniques. Among these advancements, the Common Spatial Pattern (CSP) has emerged as a widely utilized feature extraction method in EEG-based BCIs for MI classification. Originally introduced by Ramoser et al. in 2000, CSP optimally discriminates between two classes of EEG data [1].

However, CSP's performance can be compromised in high-dimensional and noisy data scenarios. To address this, several enhancements and extensions of the CSP method have been proposed. One of the most notable advancements is the Filter Bank Common Spatial Pattern (FBCSP) [13], [14] proposed by Ang et al. in 2008 and further developed in 2012. FBCSP utilizes a filter bank to decompose the EEG signal into multiple sub-bands and then applies CSP separately to each sub-band. This approach allows the extraction of frequency-specific information, resulting in a significant improvement in MI classification accuracy. Moreover, Ang et al. demonstrated the effectiveness of FBCSP on the BCI Competition IV dataset, where they achieved the highest classification accuracy [14].

The success of FBCSP sparked further exploration into optimizing the method. Thomas et al. (2009) proposed the Discriminative Common Spatial Pattern (DCSP), which integrates FBCSP with a Support Vector Machine (SVM) classifier [15]. The authors used an optimization algorithm to select the most informative frequency sub-bands, resulting in DCSP outperforming FBCSP in terms of classification accuracy.

In the quest for enhanced performance, Blankertz et al. (2008) developed an algorithm to refine the spatial filters used in FBCSP, which outperformed the standard CSP filters [16]. Additionally, Higashi and Tanaka (2013) proposed a joint optimization method for the filter bank and CSP spatial filters in FBCSP, which resulted in further enhancement of classification accuracy [17].

In terms of feature selection, Raza et al. (2015) compared various methods for FBCSP, concluding that the forward addition of frequency sub-bands achieved the highest classification accuracy [18]. Similarly, Wei and Wei (2015) proposed a Binary Particle Swarm Optimization (BPSO) algorithm for frequency sub-band selection in FBCSP, outperforming other feature selection methods [19].

Furthermore, Zhang et al. (2017) introduced Sparse Bayesian Learning (SBL), a method for obtaining sparse EEG

frequency band-based feature vectors in MI classification. They applied SBL to FBCSP and found that it outperformed other methods, including FBCSP, in terms of classification accuracy [20].

Continuing the enhancement of FBCSP, Luo et al. (2019) proposed the Class Discrepancy-Guided Sub-Band Filter-Based Common Spatial Pattern (CD-FBCSP) method, which significantly enhanced the discriminability of MI EEG signals [21].

Notably, Kumar et al. introduced the Discriminative Filter Bank Selection (DFBS) method, which outperformed the original FBCSP method by using mutual information to select the top-ranked filter banks [22]. Mammoni et al. (2023) [23] introduced an extension of the Filter Bank Common Spatial Patterns (FBCSP) algorithm, named AutoEncoder(AE)-FBCSP, to take advantage of the ability of AE to map data from the feature space to a latent space where classification-relevant information is embedded. Hwang, Park, and Chi (2023) [24] proposed a Long Short-Term Memory (LSTM)-based classification framework to enhance the classification accuracy of four-class MI signals. They used an overlapping-band-based FBCSP to extract subject-specific spatial features.

Recently, Tang et al. proposed a new spatial-frequency feature extraction method and a hybrid feature selection method for MI EEG decoding [25]. They used CSP for spatial filtering and dimensionality reduction, then decomposed the filtered signals into multiple frequency sub-bands using a filter bank. To select subject-specific spatial-frequency features, they proposed a hybrid feature selection method based on the Fisher score and SVM.

Despite the considerable advancements in the application and optimization of FBCSP, a gap remains in the consideration of overlapping frequency bands and temporal aspects of MI. Current research on optimizing FBCSP for motor imagery EEG primarily focuses on band selection and setup, advancing EEG signal classification. However, there's a notable gap regarding temporal patterns in motor imagery (MI) tasks and their interaction with overlapping frequency bands. Traditional FBCSP approaches treat EEG signals statically, ignoring evolving brain activity during tasks. This oversight hampers performance in tasks where temporal dynamics are crucial, such as distinguishing between MI tasks or detecting subtle changes over time. Additionally, overlapping frequency bands further complicate the analysis, as motor imagery tasks can activate multiple bands simultaneously. Existing methodologies often assume non-overlapping bands or use limited techniques to handle overlap, missing the richness of neural dynamics. Our proposed method addresses these gaps by integrating temporal aspects and overlapping bands into feature extraction. Through a combined block technique with FBCSP, our approach aims to enhance classification accuracy, bridging gaps in understanding and pushing BCI technology forward.

III. METHODOLOGY

1) *Dataset-Stroke Patients*: The dataset is from Clinical Brain-Computer Interfaces Challenge that was held at the

2020 IEEE World Congress on Computational Intelligence (WCCI) in Glasgow, Scotland [26]. The dataset for MI EEG classification contains .mat files, and each training file contains two variables, "rawdata" and "labels". The "rawdata" variable is a 3-D matrix that represents the activity of 12 EEG channels during 80 trials of 8 seconds each, recorded at a sampling rate of 512 Hz. The "labels" variable is a 1-D array containing the labels for individual trials in the training data, with two classes namely "left motor attempt" and "right motor attempt".

Each trial period in the calibration phase was of 8 seconds, within which the first three seconds were the preparatory phase, followed by a beep sound and a cue in the form of a hand image on the screen. Participants were instructed to perform a motor-attempt task of left or right-hand grasp based on the appearance of the cue. The scalp EEG was recorded with 12 electrodes covering specific areas, and the signals were initially filtered with a 0.1 to 100 Hz pass-band filter and a notch filter at 50 Hz during data acquisition [26].

A. Dataset-B: Healthy Subjects' Dataset

The BCI Competition IV-2a dataset has been used to compare the classification results of healthy individuals performing MI tasks [27]. This dataset has been referred to as Dataset-B for the rest of the paper. Nine healthy subjects performed MI tasks on four body parts: left hand, right hand, feet, and tongue. The training and test sessions were recorded for each subject on separate days. There were 72 trials for each class, i.e., 288 total trials per subject. Signals are sampled at a frequency of 250 Hz with an initial bandpass filter between 0.5 Hz and 100 Hz with a notch filter at 50 Hz. There were 22 Ag/AgCl electrodes following the 10-20 international system with a 3.5 cm inter-electrode distance. A trial lasts for 6 s, followed by a short break period. A fixation cross and an auditory warning were given during the first 2 s from the start of the trial. After that, a cue was presented with an arrow sign to instruct different MI tasks. Our algorithm uses the left- and right-hand MI trials as classes for our binary classification problem. This selection is made as we intend to study the performance of the classification pipeline for an upper limb motor task.

B. Pre-Processing & Feature Extraction

The methods proposed in this paper have been summarized in Fig. 1. After taking into account the buffer effect and identifying the relevant portion of the trial that corresponds to the motor imagery (MI) phase, we created the temporal blocks from the raw data, and then FBCSP was applied with mutual information (MI) based feature selection. Next, the 3 variants of the proposed method were formed such as M1, M2, and M3. The M1 variant classifies the features using a random forest algorithm without any post-processing. In contrast, a temporal probability fusion (TPF) was applied as a post-processing step for M2 while in the case of M3, we have used probability difference-based temporal fusion. All these techniques associated with M1, M2, and M3 are now explained in detail as follows.

1) *Temporal Block Approach*: The block-based temporal analysis method focuses on partitioning the time-series signal into manageable and contiguous segments or blocks. This



Fig. 1. Processing steps of Method 1 (M1), Method 2 (M2) and Method 3 (M3).

segmentation allows for a detailed examination of each separate block, potentially unveiling short-lived patterns within the signal which could be overlooked in a complete signal analysis.

The implementation of this block-based temporal analysis involves the segmentation of the time-series signal into N distinct blocks, each possessing a length L . It's important to note that L is typically much less than the full signal length. The formulation for these blocks can be mathematically represented as:

$$Block_i = [y((i-1) \cdot T + 1), y((i-1) \cdot T + 2), \dots, y((i-1) \cdot T + L)] \quad (1)$$

In this equation, y represents the time-series signal, T denotes the stepping size (which refers to the distance between consecutive blocks), and i is a counter ranging from 1 to N . It's worth noting that the signal's indices are shifted by a factor of T for each subsequent block, resulting in the creation of overlapping blocks. To be specific, we have considered data starting from 3.5 s to the end of the trial at 8s, having a window size of 1 s and a shift of 125 ms between two consecutive windows. A buffer period of 500 ms after the cue was used to prevent any edge artifacts.

2) *Filter Bank Common Spatial Pattern*: Upon the application of the temporal block-based method to segment EEG signals, we proceed with the employment of the Filter Bank Common Spatial Pattern (FBCSP) [13], [14] approach. This allows for the identification of spatial patterns related to the task at hand and the corresponding frequency bands. The process can be represented as:

$$X_{block_i} = FBCSP(Block_i) \quad (2)$$

where X_{block_i} is the transformed signal for the i -th block, and FBCSP represents the filter bank common spatial pattern method applied to each block. This technique involves the

partitioning of the EEG signal into distinct frequency bands through a filter bank, subsequently employing the Common Spatial Pattern (CSP) analysis on each band to facilitate feature extraction. The CSP method serves to derive spatial filters that augment the disparities between classifiable groups in the frequency domain.

In our methodology, we implement an overlapping frequency band strategy to augment the efficiency of the FBCSP technique. The selected frequency band for analysis spans from 8 to 40 Hz, encapsulating both the mu (8-13 Hz) and beta (13-30 Hz) bands. This frequency range has demonstrated its efficacy in Motor Imagery (MI) EEG classification assignments due to its capacity to capture a broad spectrum of frequency components pertinent to motor imagery. Aiming to elevate the FBCSP method's performance, we segment the 8 to 40 Hz frequency band into sub-bands of 4 Hz each with a 2 Hz overlap. This step enables us to garner a more granular understanding of the frequency components within each band, which can enhance the precision of the classification process. By integrating the FBCSP approach with the overlap frequency band technique, we manage to extract features from the EEG data that are more discriminatory in nature. This strategy has been validated by existing literature [20], [28], confirming its ability to enhance EEG data analysis.

3) *Mutual Information*: After extracting spatial features using the CSP algorithm, we employ mutual information-based feature selection [22], [29] to enhance the discriminative power of selected CSP components. This technique measures the dependence between features and class labels and selects the most informative features for classification. The mutual information score is calculated using the following equation:

$$MI(x_i, y_j) = \sum_{(x_i, y_j)} p(x_i, y_j) \log_2 \left(\frac{p(x_i, y_j)}{p(x_i)p(y_j)} \right) \quad (3)$$

where $MI(x_i, y_j)$ is the mutual information between feature x_i and class label y_j , $p(x_i, y_j)$ is the joint probability of x_i and y_j , and $p(x_i)$ and $p(y_j)$ are the marginal probabilities of x_i and y_j , respectively. A higher mutual information score indicates that the feature provides more information about the class label [22].

CSP components are selected as per their mutual information score.

C. Method 1 (M1)

Upon the application of the FBCSP algorithm and mutual information for spatial feature extraction and selection, the ensuing step involves feeding the chosen CSP components into a classifier. In our study, we selected the Random Forest (RF) as the classifier of choice.

RF [30] functions as an ensemble learning technique, generating numerous decision trees during its training phase and presenting the class that corresponds to the mode of the classes from the individual trees. The utilization of an ensemble of trees fosters superior generalization capabilities in contrast to a single decision tree. RF can mitigate overfitting, thereby enhancing the precision of the classification outcomes.

In the course of its training phase, RF generates a forest of decision trees, each employing a random subset of input features at each node. This strategy assists in decreasing the correlation among the trees, thereby improving the comprehensive performance of the forest. Furthermore, RF employs bootstrap aggregating (also known as bagging) to create multiple datasets by resampling the training set with replacement. Each dataset is subsequently used to train a decision tree, which is added to the forest.

The final classification decision is the culmination of aggregating the predictions from all the decision trees within the forest. In Method M1, the RF classifier is trained using feature vectors derived post the application of FBCSP and mutual information-based feature selection techniques. This trained RF classifier is then employed to predict the class labels of the testing data.

D. Method 2 (M2)

Method 2 (M2) extends the classification strategy employed in Method 1 by integrating a temporal probability Fusion mechanism, which takes into account the model's uncertainty about its predictions.

1) *Temporal Probability Fusion*: In the Temporal Probability Fusion (TPF) approach, classification decisions are made based on the weighted sum of prediction probabilities across all temporal blocks belonging to a single trial. This approach is particularly useful for EEG-based motor imagery tasks with two classes, such as left-hand movement and right-hand movement.

The approach can be summarized as follows: First, obtain the prediction probabilities for each temporal block using a classifier, such as a Random Forest. For each block, the classifier outputs a probability for each class (in this case, left-hand movement and right-hand movement). Next, for each trial, compute the weighted sum of prediction probabilities for each class across all temporal blocks. The weighted sum for class i ($i \in 1, 2$) can be computed as:

$$W_i = \sum_{j=1}^n (P_{ij} \cdot w_j) \quad (4)$$

where W_i is the weighted sum for class i , P_{ij} is the probability of class i in the j -th temporal block, w_j is the weight assigned to the j -th temporal block, and n is the number of temporal blocks. It is to be noted that we assign equal weights to all blocks within a trial. Each block contributes equally to the combined prediction probabilities for each class. We made this design choice to ensure simplicity and consistency in the fusion process as we aim to give importance to all blocks without introducing bias based on their position.

Finally, for each trial, assign the class with the highest weighted sum as the predicted class label. Calculate the accuracy of the TPF approach by comparing the predicted class labels to the true class labels.

The TPF approach is advantageous because it takes into account the prediction probabilities from all temporal blocks, allowing the classifier to leverage the most informative features

across time. By incorporating the prediction probabilities in a weighted manner, the TPF method can potentially improve the classification performance compared to considering only the most discriminative temporal block or using a simple majority vote.

E. Method 3 (M3)

Method 3 (M3) builds on the classification approach used in Method 1 by incorporating probability difference-based temporal fusion, which considers the model's ambivalence in its prediction outcomes.

1) *Probability Difference-based Temporal Fusion*: In the Probability Difference-based Temporal Fusion (PDTF) approach, the goal is to classify trials into one of two classes: left-hand movement or right-hand movement. This is achieved by considering the differences in prediction probabilities across all temporal blocks within a single trial and fusing them together to make the final classification decision.

Let's break down the PDTF approach used in the provided code with mathematical details:

For each instance in the test set, obtain the prediction probabilities using the classifier model:

$P(C1|x_i)$: Probability of instance x_i belonging to class 1 (left-hand movement)

$P(C2|x_i)$: Probability of instance x_i belonging to class 2 (right-hand movement)

Calculate the probability difference for each instance in the test set:

$$D(x_i) = P(C1|x_i) - P(C2|x_i) \quad (5)$$

Assign the class label for each instance based on the probability difference:

If $D(x_i) > 0$, assign class label 1 (left-hand movement)

If $D(x_i) < 0$, assign class label 2 (right-hand movement)

If $D(x_i) = 0$, use the previous instance's class label

For each trial, aggregate the probability differences across all temporal blocks:

$$A_k = \sum_{j=1}^n D_{kj} \quad (6)$$

Where A_k is the aggregated probability difference for trial k , n is the number of temporal blocks in a trial, and D_{kj} is the probability difference for temporal block j in trial k .

Make the final class label decision for each trial based on the aggregated probability differences:

If $A_k > 0$, assign class label 1 (left-hand movement)

If $A_k < 0$, assign class label 2 (right-hand movement)

The connection between formulas (5) and (6) becomes evident when we consider that the individual probability differences ($D(x_i)$) calculated using equation (5) for each instance becomes the basis for the probability differences (D_{kj}) in equation (6) which are then calculated for each block within a trial. By summing these temporal probability differences, we obtain A_k , which represents the aggregated probability difference, for the trial.

In order to make informed decisions around class labels, capturing temporal information is key. The PDTF approach does just that by aggregating probability differences across all temporal blocks within a trial, effectively incorporating timing into its final classification decision. This technique could prove especially useful when dealing with complex data sets where capturing nuances in timing can make all the difference.

IV. RESULT & DISCUSSION

To gain insight into hand functional disability following hemiparetic stroke, we conducted a study on a sample of 10 patients. To collect data, we observed participants as they attempted grasp movements using both their left and right hands while EEG recordings were taken. We only used the training files for analysis as the labels for the original evaluation files were not known to us.

To evaluate our system's capabilities, we employed a rigorous method known as 5-fold cross-validation on our dataset. This meant that we fragmented it into five identical pieces with only one section being used for verification purposes every time while others confined themselves to training duties alternately. By measuring performance metrics in each fold and subsequently combining them together using averages, a general overview accurately encapsulates how proficiently our model functions.

Incorporating 5-fold cross-validation into research methodology presents numerous benefits including minimizing variation, optimizing hyperparameters, and delivering a more precise gauge of the effectiveness of a model. Within the research community, this approach has gained traction for assessing models.

A. Model Evaluation

1) *Channel Selection Analysis and Implications*: Achieving optimal performance in EEG-based motor imagery (MI) classification is heavily dependent on the proper selection of EEG channels. Our study investigates the impact of channel selection on the classification accuracy of these methods: M1, M2 (Temporal Probability Fusion, TPF), and M3 (Probability Difference-based Temporal Fusion, PDTF).

We first examined how the classification accuracy varied with the number of channels used. Specifically, we considered subsets of 3, 5, 6, 9, and 12 channels selected based on their mutual information. The results indicate that the mean accuracy for M1, M2, and M3 methods generally improved as the number of channels increased as shown in Fig. 2. M1 demonstrated mean accuracies of 0.6571, 0.7112, 0.6994, 0.7163, and 0.7437, and M2 has accuracies of 0.7589, 0.7849, 0.792, 0.816, and 0.8579, while M3 showed accuracies of

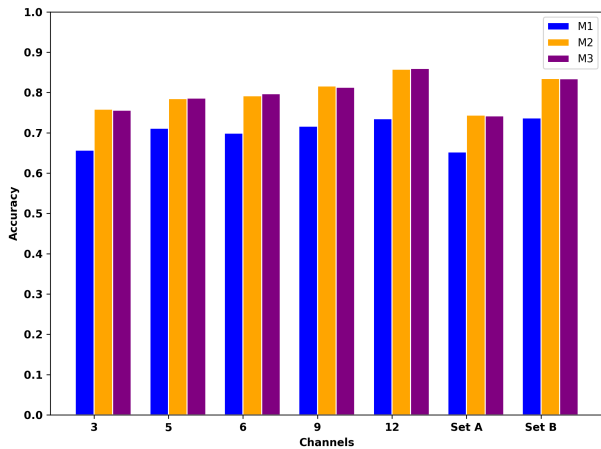


Fig. 2. Channel-wise accuracy comparison of three methods: M1, M2, and M3.

0.756, 0.786, 0.7969, 0.813, and 0.8599 for 3, 5, 6, 9, and 12 channels, respectively.

It's becoming increasingly clear that adopting a wider range of channels to record motor cortex activity during MI tasks is crucial. This trend supports the notion that enhancing classification accuracy requires capturing a more comprehensive view of the activity at play.

We then considered two specific sets of channels, Set A (C3, C4, CPz) and Set B (F3, FC3, C3, CP3, P3, F4, FC4, C4, CP4), which have been associated with MI EEG of the left and right hand [31], [32]. The M1 method achieved mean accuracies of 0.6527 and 0.7369 for Set A and Set B respectively, M2 achieved 0.744 and 0.835 for Set A and Set B respectively, while the M3 method showed mean accuracies of 0.742 and 0.834 for Set A and Set B respectively.

The improved performance of the methods with Set B corroborates the importance of including more channels for higher accuracy. The channels in Set B, which span a broader area of the motor cortex, provide a more comprehensive view of the neural activity, facilitating more accurate differentiation between left and right-hand MI tasks.

However, the slight edge of M2 over M3 for both channel sets suggests that the TPF approach, with its probability-Fusion mechanism, might be slightly more effective in handling the spatial information from multiple channels.

B. Overlap Size and its Impact

When analyzing EEG signals, it's important to consider the element of time. The patterns found in EEG signals are complex and understanding them is key to comprehending brain activity. Scientists have developed two approaches to aid in this understanding: TPF assigns weights based on temporal occurrence while PDTF harnesses the model's uncertainty through differences in class probabilities. This differential approach can be considered an indirect measure of the signal's temporal information, and it provides a potentially more sophisticated representation of the temporal dynamics.

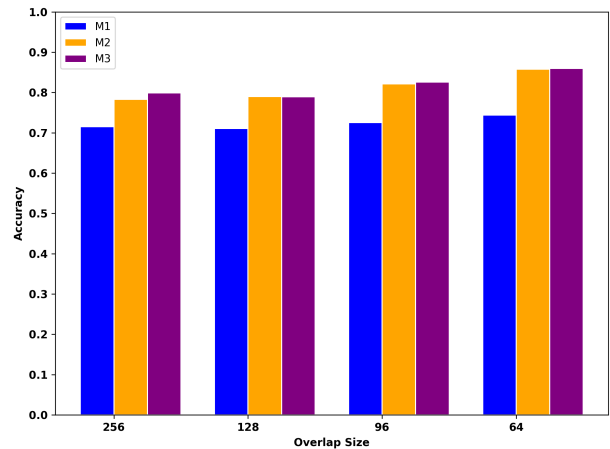


Fig. 3. Overlap size-wise accuracy comparison of three methods: M1, M2, and M3.

The performance of M1, M2, and M3 methods was evaluated under various overlap sizes in temporal blocks, namely, 256, 128, 96, and 64 with all 12 channels as shown in Fig. 3.

The relationship between overlap size and classification accuracy is intricate and demands deliberate analysis. Including the right degree of overlap is vital as it keeps signal continuity and context intact. Nonetheless, it's essential to recognize that there exists an ideal threshold for overlap beyond which advantages diminish, leading to probable drawbacks like redundancy and overfitting. On the other hand, inadequate overlap may not maintain the temporal dependencies intrinsic in EEG signals effectively, consequently affecting classifier performance.

In our study, an overlap size of 64 exhibited superior results with both Temporal Probability Fusion (TPF) and Probability Difference-based Temporal Fusion (PDTF) techniques. This suggests that the judicious selection of overlap size plays a critical role in improving the classification performance. A discernible trend is a rise in accuracy scores as the overlap size decreases, potentially due to the introduction of more distinguishable features that can enhance the differentiation of left and right motor imagery EEG signals.

It's also worth noting that PDTF (M3) consistently outperformed TPF (M2) across varying overlap sizes, exhibiting particularly pronounced advantages as the overlap size decreased. This could indicate that PDTF is more adaptable to fluctuations in overlap size. The difference in performance might be attributed to PDTF's sensitivity to changes in temporal structure, allowing it to more effectively leverage the variation in features introduced by different overlap sizes.

C. Overall Comparison of Methods

We compared the accuracies of methods M1, M2, and M3 as shown in Table I. In our Random Forest (RF) criterion selection process, we delved into two distinct criteria: 'gini' and 'entropy,' in order to assess their influence on the model's performance. As for the determination of the number of trees in the Random Forest ensemble, we conducted experiments using three different values: 100, 150, and 200. Concerning

the maximum depth of each individual decision tree within the Random Forest ensemble, we conducted tests with three depth values: 10, 20, and 30. Once we completed this grid search we carefully analyzed the results obtained. Our findings revealed that using 'entropy' as the criterion while setting the Number of Estimators to 200 and Maximum Depth to 20 yielded maximum accuracy, for our classification task. M2 achieved an accuracy of 85.5% while M3 achieved an accuracy of 85.4%.

TABLE I
CLASSIFICATION ACCURACIES FOR M1, M2, AND M3 METHODS FOR THE STROKE PATIENTS' DATASET AFTER RF PARAMETER TUNING AND COMPARISON WITH FBCNET. THE *Cohen's-d* VALUES AT THE BOTTOM ROW SHOW THE COMPARISON OF EACH METHOD WITH M1

SubID	Accuracy (%)			FBCNet
	M1 (FBCSP)	M2 (M1+TPF)	M3 (M1+PDTF)	
P01	83.56	98.00	97.00	85
P02	83.92	85.00	87.00	92.5
P03	79.52	80.00	81.00	82.5
P04	80.84	98.00	96.00	87.5
P05	83.4	91.00	90.00	85
P06	85.08	87.00	87.00	88.75
P07	82.2	79.00	79.00	83.75
P08	77.84	81.00	80.00	91.25
P09	77.96	67.00	67.00	66.25
P10	82.32	89.00	90.00	87.5
Mean	81.664	85.50	85.40	85
Std	2.53	9.38	8.96	7.31
<i>Cohen's-d</i>		0.53	0.59	0.58

TABLE II
CLASSIFICATION ACCURACIES FOR M2, AND M3 METHODS FOR BCI COMPETITION IV-2A DATASET AND COMPARISON WITH OTHER METHODS. THE *Cohen's-d* VALUES AT THE BOTTOM ROW SHOW THE COMPARISON OF EACH METHOD WITH M2 OR M3

SubID	Accuracy(%)				
	M2	M3	SW-LCR	SS-MEMDBF	EEG-CSAC
A01	88.19	88.19	86.81	91.49	90.28
A02	70.49	70.49	64.58	60.56	57.64
A03	88.54	88.89	95.83	94.24	95.14
A04	90.28	90.63	67.36	76.72	65.97
A05	89.24	90.28	68.06	58.52	61.11
A06	80.56	81.60	67.36	68.52	65.28
A07	79.17	79.51	80.56	78.57	61.11
A08	93.40	92.71	97.22	97.01	91.67
A09	91.67	90.97	92.36	93.85	86.11
AVG	85.73	85.92	80.02	79.94	74.92
Std	7.44	7.29	13.45	15.00	15.43
<i>Cohen's-d</i>			0.5	0.46	0.85

We can also observe from Table I that the performance of M2 (average CA 85.5%) and M3 (average CA 85.4%) is higher (the *Cohen's d* value of 0.53 and 0.59 shows a moderate to high effect size for these comparisons) than M1 or FBCSP (average CA 81.66%) by more than 3.7% while as compared to FBCNet [33] (average CA 85%) their performance is found to be comparable. Apart from the higher accuracy, another advantage of using M2 and M3 methods is that, unlike the deep learning methods, the extracted features are more interpretable as they are statistical and also it would require much less

computational resources to implement and deploy. We also observed that incorporating the difference in classification probabilities through PDTF might boost effectiveness for some subjects as compared to M2. Notably, subjects 1, 5, 6, and 8 display particularly compelling results within this context as they got higher accuracy in M3 than in M2. Overall, taking into account nuanced indicators of decision-making processes appears to offer higher levels of accuracy.

It should be noted that although PDTF typically leads to superior results when compared with TPF methodologically speaking, this does not hold true across all test subjects. In specific instances such as subjects 2, 7, and 10, the performances of both methods prove largely similar. In fact, PDTF appears to lead to negative outcomes (compared with TPF) for subjects 3,4, and 9 in this particular study. These discrepancies may be connected with differences in each individual's brain signals as well as their alignment with one strategy or the other.

Our investigation delved deeper into the competency of Methods M1, M2, and M3 against other leading techniques. In 2021, the results of the CBCIC 2020 were published with a ranked list of methods that yielded the highest accuracies in the competition [26]. The winner in the within-subject category achieved an average accuracy of 78.44% using Riemannian manifold + functional connectivity-based features and ensemble learning. In contrast, the proposed M2 and M3 methods outperformed this approach significantly, achieving average accuracies of 87.37% and 86.75%, respectively. Worth noting is that both M2 and M3 are considerably simpler than the competition's winning method, leading to reduced computational complexity and easier implementation. Another notable method for classifying motor imagery signals in the past two years is the sliding window CSP with longest consecutive repetition (SW-LCR) published in 2021 [10]. The average classification accuracy achieved by SW-LCR for the CBCIC 2020 dataset was 73.5%, significantly lower than the accuracy achieved by M2 and M3. Subsequently, in 2023, the sliding window technique was combined with the popular EEGNet-based deep learning architecture (SW-EEGNet) for motor imagery classification and was tested on the same CBCIC 2020 dataset [11]. The SW-EEGNet yielded an average accuracy of 76.94%, still nearly 10% lower than that of M2 and M3. We ensured a just evaluation by employing datasets P01 to P08 that were formerly used in a benchmark publication [34]. By using these datasets, we were able to evaluate the performance of M1, M2, and M3 methods against other established approaches. The comparison was done using accuracy as a metric, and the results are illustrated in Fig. 4. The purpose of the comparison was to determine which method performs better in terms of classification accuracy and which method is more stable. We have also compared our method with a recently published paper on the same dataset which achieved an accuracy of $79.25 \pm 7.73\%$ [35]. As compared to this the proposed method (M2 and M3) achieved superior performance as the average accuracy is more than 6% higher for M2 and M3 with a moderately high effect size (*Cohen's d* = 0.74).

Additionally, we have given the results of the proposed methods of M2 and M3 on publicly available and one of

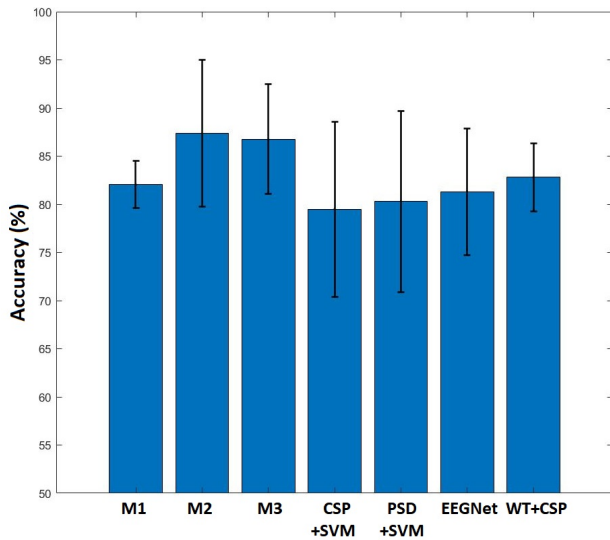


Fig. 4. A comparison of the performance between the proposed method and existing methods.

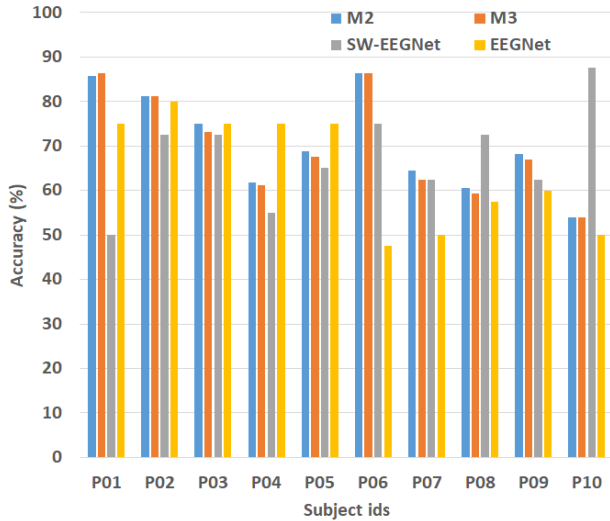


Fig. 5. Cross-subject classification accuracies for stroke patient dataset using M2 and M3 and comparison with EEGNet and SW-EEGNet.

the most popular BCIC IV 2a dataset. To keep the parity with the stroke patients dataset we have chosen the left and right motor imagery classes as a binary classification problem from BCIC IV 2a dataset. Table II describes the results and comparison with some previously published results. From Table II we can see that the average CA for M2 and M3 on BCIC IV-2a were 85.73% and 85.92% which outperformed the other competitive methods such as SW-LCR [10], SS-MEMDBF [36], and EEGCSAC [37]. For example, as compared to the multivariate empirical mode decomposition based on the Riemannian geometry-based method (SS-MEMDBF) which yielded an average CA of 79.94% the proposed M2 and M3 achieved more than 5.79% accuracy while as compared to the covariate shift adaptation technique (EEGCSAC) the increment in accuracy was more than 10.81%. We have also compared the performance of M2 and M3 on BCIC IV-2a with

the recent SW-LCR (average CA 80.02%) method where the enhancement in accuracy in favour of the proposed methods was more than 5.71%.

We have also calculated the cross-subject classification accuracies of the proposed M2 and M3 methods on the stroke patients' dataset and compared it with the previously published results on EEGNet [37] and SW-EEGNet [11] which is depicted in Fig. 5. The average classification accuracies across all the subjects for M2 and M3 were 70.18% and 69.43% respectively which outperformed the results obtained by EEGNet (average classification accuracy, 64.5%) and SW-EEGNet (67.5%) on the same dataset for inter-subject classification. Thus we can argue that the results obtained by the proposed M2 and M3 methods are promising not only in subject-specific decoding but also in cross-subject decoding.

From the statistical tests we can see that both M2 and M3 have moderately high effect sizes (Cohen's $d = 0.69$ and 0.74 respectively) when the average accuracy is compared against the recently published SCSP-3 method where M2 and M3 achieved more than 6% higher average accuracy. M2 and M3 have also significantly outperformed EEGNet with p -values 0.03 and 0.02 respectively (Cohen's $d = 1.08$ and 1.11 respectively). For the cross-subject comparisons using the stroke patients dataset M2 and M3 outperformed the recently published SW-EEGNet method with a moderate effect size of Cohen's $d = 0.49$ and 0.42 respectively. On the healthy subjects' dataset (BCI competition IV-2a) the M2 and M3 methods outperformed the previously obtained results using SW-LCR with a moderate effect size of Cohen's d more than 0.5 while the higher performance as compared to SS-MEMDBF was also observed with a moderate effect size of Cohen's d more than 0.47. The M2 and M3 methods also achieved significantly (p -value; 0.05) higher performance as compared to the EEGCSAC method with a high effect size of Cohen's $d = 0.85$.

The moving window approach coupled with CSP and SVM [13], [34] presents a different pathway for EEG signal analysis. This method incorporates a moving window to extract features from the EEG signals, enhances the relevant features via CSP filtering, and finally classifies the signals using the SVM algorithm. The extraction of time-frequency characteristics in the Wavelet Transform Common Spatial Pattern (WT-CSP) [38] method involves a dual approach. This entails utilizing wavelet transform-based decomposition techniques such as the Discrete Wavelet Transform (DWT) and Wavelet Packet Decomposition (WPD) which incorporate multistage sub-band filters that implement both high pass and low pass filtering at every stage. In contrast, the PSD with SVM [34] approach calculates the power spectral density of the EEG signals, extracts the relevant features, and then employs an SVM algorithm for classification. On the other hand, EEGNET [39], a deep learning-based method for EEG classification, uses a convolutional neural network (CNN) to learn the distinguishing features from EEG data.

In our methods, M2 has a standard deviation of 6.22, and M3 has a standard deviation of 5.20. These figures are substantially lower than those observed in the state-of-the-art methods. For instance, CSP+SVM has a standard deviation of

9.1, PSD+SVM has 9.4, and EEGNET has 6.6. Lower standard deviation in our methods signifies more consistent and reliable performance across different subjects and trials.

Our proposed methods, M2 and M3, stand out with their superior mean accuracy and improved consistency when compared to other methods. For example, the statistical test between M3 and the baseline CSP+SVM method [34]; and between M2 and the baseline CSP+SVM method [34] revealed that in both the cases the improvement in results in favour of M2 and M3 were statistically significant (p -value <0.01). Their high level of accuracy coupled with lower variability makes them highly robust and reliable in classifying MI EEG. These methods perform effectively on average and are relatively stable.

Comparatively, the M1 method, although it presents lower accuracy than others such as CSP+SVM, PSD+SVM, WT+CSP and EEGNET, exhibits a markedly lower standard deviation. This outcome implies a higher degree of stability and consistency in M1's performance across different subjects. Such a characteristic is invaluable in practical applications where the predictability of the system's behavior is critical [40].

V. CONCLUSION

In order for BCI systems to achieve their desired outcomes, accurate classifications of MI tasks are critical. The reason is that how well a system can interpret brain signals determines its ability to transform them into understandable actions. Developing EEG classification methods that are both dependable and precise when it comes to capturing these signals is therefore paramount. Such advancements will strengthen the potential for wider implementation and efficacy across different domains including neurorehabilitation.

Our proposed method, M1 used a temporal block approach on the EEG data, followed by Filter Bank Common Spatial Pattern (FBCSP) with an overlap frequency band, feature selection with the highest mutual information, and Random Forest as a classifier. The TPF (M2) method, with its emphasis on probability-weighted decision-making, proved to be adept at handling the spatial information gleaned from multiple channels. Conversely, the PDTF(M3) method focused on leveraging model uncertainty and showcased robustness in situations where model predictions are ambiguous. Through experiments, we demonstrated that our proposed methods outperformed existing methods in classifying MI EEG data from subjects.

Although the results are promising, it's crucial to acknowledge that there's still ample room for further advancement and investigation. To enhance outcomes, upcoming studies could employ sophisticated machine learning and deep learning models, experiment with hybrid methods that merge the strengths of TPF and PDTF, and devise adaptive approaches for overlap size and channel selection. Deep learning models, such as Convolutional Neural Networks (CNNs) and Recurrent Neural Networks (RNNs), could be particularly effective due to their ability to handle temporal sequences and high-dimensional data, which are inherent to EEG signals

although the need for large training data is always a problem for deep learning as it is time-consuming to record [41]. Additionally, exploring different kinds of EEG signals like cognitive tasks related ones or those associated with sleep stages or emotions through the use of TPF and PDTF methods could be an interesting avenue for research. Moreover, it would be intriguing to test the validity of applying these techniques in real-time situations - especially concerning their usage within Brain-Computer Interface (BCI) systems designed for neurorehabilitation purposes or gaming-related activities like virtual reality experiences.

REFERENCES

- [1] H. Ramoser, J. Müller-Gerking, and G. Pfurtscheller, "Optimal spatial filtering of single trial eeg during imagined hand movement," *IEEE Transactions on Rehabilitation Engineering*, vol. 8, no. 4, pp. 441–446, 2000.
- [2] J. R. Wolpaw and et al., "Brain-computer interface technology: A review of the first international meeting," *IEEE Transactions on Rehabilitation Engineering*, vol. 8, no. 2, pp. 164–173, 2000.
- [3] T. Koceljko, N. Matuszkiewicz, P. Durawa, A. Madajczak, and J. Kwiatkowski, "How integration of a brain-machine interface and obstacle detection system can improve wheelchair control via movement imagery," *Sensors*, vol. 24, no. 3, 2024.
- [4] L. Chen, P. Chen, S. Zhao, Z. Luo, W. Chen, Y. Pei, H. Zhao, J. Jiang, M. Xu, Y. Yan, and E. Yin, "Adaptive asynchronous control system of robotic arm based on augmented reality-assisted brain-computer interface," *Journal of Neural Engineering*, vol. 18, no. 6, p. 066005, nov 2021.
- [5] L. Bi, J. Lian, K. Jie, R. Lai, and Y. Liu, "A speed and direction-based cursor control system with p300 and ssvep," *Biomedical Signal Processing and Control*, vol. 14, pp. 126–133, 2014.
- [6] K. Lafleur, K. Cassady, A. Doud, K. Shades, E. Rogin, and B. He, "Quadcopter control in three-dimensional space using a noninvasive motor imagery-based brain-computer interface," *Journal of Neural Engineering*, vol. 10, no. 4, 2013.
- [7] F. Pichiorri, N. Mrachacz-Kersting, M. Molinari, S. Kleih, A. Kübler, and D. Mattia, "Brain-computer interface based motor and cognitive rehabilitation after stroke – state of the art, opportunity, and barriers: summary of the bci meeting 2016 in asilomar," *Brain-Computer Interfaces*, vol. 4, no. 1–2, pp. 53–59, Apr. 2017.
- [8] C. Zuo *et al.*, "Novel hybrid brain-computer interface system based on motor imagery and p300," *Cognitive Neurodynamics*, vol. 14, no. 2, pp. 253–265, Apr. 2020.
- [9] F. Lotte, "A tutorial on eeg signal-processing techniques for mental-state recognition in brain-computer interfaces," in *Guide to Brain-Computer Music Interfacing*. Springer London, 2014, pp. 133–161.
- [10] P. Gaur, H. Gupta, A. Chowdhury, K. McCreadie, R. B. Pachori, and H. Wang, "A sliding window common spatial pattern for enhancing motor imagery classification in eeg-bci," *IEEE Transactions on Instrumentation and Measurement*, vol. 70, pp. 1–9, 2021.
- [11] P. Saideepthi, A. Chowdhury, P. Gaur, and R. B. Pachori, "Sliding window along with eegnet-based prediction of eeg motor imagery," *IEEE Sensors Journal*, vol. 23, no. 15, pp. 17703–17713, 2023.
- [12] J. Jiang, C. Wang, J. Wu, W. Qin, M. Xu, and E. Yin, "Temporal combination pattern optimization based on feature selection method for motor imagery bcis," *Frontiers in Human Neuroscience*, vol. 14, 2020.
- [13] K. K. Ang, Z. Y. Chin, H. Zhang, and C. Guan, "Filter bank common spatial pattern (fbcs) in brain-computer interface," in *2008 IEEE International Joint Conference on Neural Networks (IEEE World Congress on Computational Intelligence)*, Jun. 2008, pp. 2390–2397.
- [14] Z. H. A. K. Keng, C. Z. Yang, W. Chuanchu, and G. Cuntai, "Filter bank common spatial pattern algorithm on bci competition iv datasets 2a and 2b," *Frontiers in Neuroscience*, vol. 6, 2012.
- [15] K. P. Thomas, C. T. Lau, A. P. Vinod, C. Guan, and K. K. Ang, "A new discriminative common spatial pattern method for motor imagery brain-computer interfaces," *IEEE Transactions on Biomedical Engineering*, vol. 56, no. 11, pp. 2730–2733, 2009.
- [16] B. Benjamin, T. Ryota, L. Steven, K. Motoaki, and M. Klaus-Robert, "Optimizing spatial filters for robust eeg single-trial analysis," *IEEE Signal Processing Magazine*, vol. 25, pp. 41–56, 2008.

- [17] H. Higashi and T. Tanaka, "Simultaneous design of fir filter banks and spatial patterns for eeg signal classification," *IEEE Transactions on Biomedical Engineering*, vol. 60, no. 4, pp. 1100–1110, Apr. 2013.
- [18] H. Raza, H. Cecotti, and G. Prasad, "Optimising frequency band selection with forward-addition and backward-elimination algorithms in eeg-based brain-computer interfaces," in *2015 International Joint Conference on Neural Networks (IJCNN)*, Jul. 2015, pp. 1–7.
- [19] Q. Wei and Z. Wei, "Binary particle swarm optimization for frequency band selection in motor imagery based brain-computer interfaces," *Biomedical Materials and Engineering*, vol. 26, no. s1, pp. S1523–S1532, Aug. 2015.
- [20] Y. Zhang, Y. Wang, J. Jin, and X. Wang, "Sparse bayesian learning for obtaining sparsity of eeg frequency bands based feature vectors in motor imagery classification," *International Journal of Neural Systems*, vol. 27, no. 2, 2017.
- [21] L. J., W. J., X. R., and X. K., "Class discrepancy-guided sub-band filter-based common spatial pattern for motor imagery classification," *Journal of Neuroscience Methods*, vol. 323, pp. 98–107, 2019.
- [22] S. Kumar, A. Sharma, and T. Tsunoda, "An improved discriminative filter bank selection approach for motor imagery eeg signal classification using mutual information," *BMC Bioinformatics*, vol. 18, no. S16, p. 545, Dec. 2017.
- [23] N. Mammone, C. Ieracitano, H. Adeli, and F. C. Morabito, "Autoencoder filter bank common spatial patterns to decode motor imagery from eeg," *IEEE Journal of Biomedical and Health Informatics*, vol. 27, no. 5, pp. 2365–2376, May 2023.
- [24] J. Hwang, S. Park, and J. Chi, "Improving multi-class motor imagery eeg classification using overlapping sliding window and deep learning model," *Electronics*, vol. 12, no. 5, p. 1186, Mar. 2023.
- [25] Y. Tang, Z. Zhao, S. Zhang, Z. Li, Y. Mo, and Y. Guo, "Motor imagery eeg decoding based on new spatial-frequency feature and hybrid feature selection method," *Mathematical Problems in Engineering*, vol. 2022, pp. 1–12, Jan. 2022.
- [26] A. Chowdhury and J. Andreu-Perez, "Clinical brain-computer interface challenge 2020 (cbci at wcci2020): Overview, methods, and results," *IEEE Transactions on Medical Robotics and Bionics*, Oct. 2021.
- [27] M. Tangermann *et al.*, "Review of the bci competition iv," *Frontiers in Neuroscience*, vol. 6, 2012.
- [28] K.-T. Kim, J. Lee, H. Kim, C. H. Kim, and S. J. Lee, "Classification of selective attention within steady-state somatosensory evoked potentials from dry electrodes using mutual information-based spatio-spectral feature selection," *IEEE Access*, vol. 8, pp. 85 464–85 472, 2020.
- [29] K. K. Ang, Z. Y. Chin, H. Zhang, and C. Guan, "Mutual information-based selection of optimal spatial-temporal patterns for single-trial eeg-based bcis," *Pattern Recognition*, vol. 45, no. 6, pp. 2137–2144, 2012.
- [30] L. Breiman, "Random forests," *Machine Learning*, vol. 45, no. 1, pp. 5–32, 2001.
- [31] Z. Ma, K. Wang, M. Xu, W. Yi, F. Xu, and D. Ming, "Transformed common spatial pattern for motor imagery-based brain-computer interfaces," *Frontiers in Neuroscience*, vol. 17, Mar. 2023.
- [32] B. Xu *et al.*, "Wavelet transform time-frequency image and convolutional network-based motor imagery eeg classification," *IEEE Access*, vol. 7, pp. 6084–6093, 2019.
- [33] R. Mane, N. Robinson, A. P. Vinod, S.-W. Lee, and C. Guan, "A multi-view cnn with novel variance layer for motor imagery brain computer interface," in *2020 42nd Annual International Conference of the IEEE Engineering in Medicine & Biology Society (EMBC)*, 2020, pp. 2950–2953.
- [34] S. Rasheed and W. Mumtaz, "Classification of hand-grasp movements of stroke patients using eeg data," in *2021 International Conference on Artificial Intelligence (ICAI)*, Apr. 2021, pp. 86–90.
- [35] S. Khanna, A. Chowdhury, A. Dutta, and V. K. Subramanian, "Scsp-3: A spectrally augmented common spatial pattern approach for robust motor imagery-based brain-computer interface," *IEEE Sensors Journal*, pp. 1–1, 2024.
- [36] P. Gaur, R. B. Pachori, H. Wang, and G. Prasad, "A multi-class eeg-based bci classification using multivariate empirical mode decomposition based filtering and riemannian geometry," *Expert Systems with Applications*, vol. 95, pp. 201–211, 2018.
- [37] H. Raza, A. Chowdhury, S. Bhattacharyya, and S. Samothrakis, "Single-trial eeg classification with eegnet and neural structured learning for improving bci performance," in *2020 International Joint Conference on Neural Networks (IJCNN)*, 2020, pp. 1–8.
- [38] J. Kevric and A. Subasi, "Comparison of signal decomposition methods in classification of eeg signals for motor-imagery bci system," *Biomedical Signal Processing and Control*, vol. 31, pp. 398–406, Jan. 2017.
- [39] V. J. Lawhern, A. J. Solon, N. R. Waytowich, S. M. Gordon, C. P. Hung, and B. J. Lance, "Eegnet: A compact convolutional neural network for eeg-based brain-computer interfaces," *Journal of Neural Engineering*, vol. 15, no. 5, p. 056013, Oct. 2018.
- [40] Y. Pei, Z. Luo, H. Zhao, D. Xu, W. Li, Y. Yan, H. Yan, L. Xie, M. Xu, and E. Yin, "A tensor-based frequency features combination method for brain-computer interfaces," *IEEE Transactions on Neural Systems and Rehabilitation Engineering*, vol. 30, pp. 465–475, 2022.
- [41] Y. Pei, Z. Luo, Y. Yan, H. Yan, J. Jiang, W. Li, L. Xie, and E. Yin, "Data augmentation: Using channel-level recombination to improve classification performance for motor imagery eeg," *Frontiers in Human Neuroscience*, vol. 15, 2021.